Carborane Clusters in Computational Drug Design: A Comparative Docking Evaluation Using AutoDock, FlexX, Glide, and Surflex

Rohit Tiwari,*[,†] Kiran Mahasenan,[†] Ryan Pavlovicz,[‡] Chenglong Li,[†] and Werner Tjarks*[,†]

Division of Medicinal Chemistry & Pharmacognosy, College of Pharmacy and Biophysics Program, The Ohio State University, Columbus, Ohio 43210

Received January 23, 2009

Compounds containing boron atoms play increasingly important roles in the therapy and diagnosis of various diseases, particularly cancer. However, computational drug design of boron-containing therapeutics and diagnostics is hampered by the fact that many software packages used for this purpose lack parameters for all or part of the various types of boron atoms. In the present paper, we describe simple and efficient strategies to overcome this problem, which are based on the replacement of boron atom types with carbon atom types. The developed methods were validated by docking *closo*- and *nido*-carboranyl antifolates into the active site of a human dihydrofolate reductase (hDHFR) using AutoDock, Glide, FlexX, and Surflex and comparing the obtained docking poses with the poses of their counterparts in the original hDHFR-carboranyl antifolate crystal structures. Under optimized conditions, AutoDock and Glide were equally good in docking of the *closo*-carboranyl antifolates followed by Surflex and FlexX, whereas Autodock, Glide, and Surflex proved to be comparably efficient in the docking of *nido*-carboranyl antifolates followed by FlexX. Differences in geometries and partial atom charges in the structures of the carboranyl antifolates resulting from different data sources and/or optimization methods did not impact the docking performances of AutoDock or Glide significantly. Binding energies predicted by all four programs were in accordance with experimental data.

INTRODUCTION

Chemical, physicochemical, and structural versatility combined with high stability under physiological conditions are distinctive features of carboranes and other boron clusters.[1,2] They have been used for decades in the design and synthesis of therapeutics for Boron Neutron Capture Therapy (BNCT) of cancer and, more recently, in other areas of drug design.[1,2] Hydrophobic *closo*-carboranes, comparable in dimensions to adamantane,[3] were used as bioisosteric replacements for (hetero)aromatic and (hetero)aliphatic ring systems and other bulky entities in the design and synthesis of carboranyl derivatives of various amino acids and peptides,[2] estrogen receptor modulators,[4] androgen receptor antagonists,[5] retinoids,[3] benzolactamic protein kinase C inhibitors,[6] thalidomide,[7] flufenamic acid,[8] diflunisal,[8] thrombin inhibitors,[9] and trimethoprim.[10] Many of these boronated derivatives displayed biological activities comparable or even superior to those of their nonboronated counterparts. In a different type of application, negatively charged boron clusters have been utilized as "prosthetic groups" for radiohalogens in the design and synthesis of radiotherapeutics and imaging agents.[11,12] These types of cages are readily halogenated, and the boron-halogen bonds within these structures appear to be less susceptible to *in vivo* cleavage than carbon−halogen bonds.[11,12] In addition, metallocarboranes were found to be effective inhibitors of HIV-1 protease,[13] and therapeutics containing single boron atoms, such as the proteasome inhibitor bortezomib,[14] have attracted considerable attention in recent years.

Drug design involving boron-containing agents has two major disadvantages compared with conventional drug design: (1) there is a lack of compound libraries containing boron agents for virtual screening,[15] and (2) many software packages available for structure/ligand-based drug design do not have inbuilt parameters for boron. Several strategies to circumvent the latter problem have been reported in recent years. These include the substitution of boron with carbon[16−19,21,22] and the calculation of suitable boron parameter for specific applications.[20] Other reports dealing with docking studies of boron compounds do not provide specific information on computational strategies addressing this problem.[9,23,24]

Crystal structures of proteins complexed with carborane-containing agents, including those of *closo*- and *nido*-carboranyl antifolates with human dihydrofolate reductase (hDHFR), have been reported recently.[10,13] These provide for the first time the opportunity to verify docking strategies that have been previously developed for carboranyl compounds.[17] In the present paper, we evaluate the docking of these carboranyl antifolates into the active site of the hDHFR crystal structures using the docking programs AutoDock, Glide, FlexX, and Surflex. The computationally determined docking poses are compared with the poses of the corresponding carboranyl antifolates in the original hDHFR crystal structures, and differences between the docking programs are discussed. The described computational studies will be of great interest for scientists involved in the design and development of boron-containing therapeutics and diagnostics who have had very limited access to computational tools in the past.

* Corresponding author phone: (614)688-3149; e-mail: tiwari.13@osu.edu (R.T.); phone: (614)292-7624; e-mail: tjarks.1@osu.edu (W.T.).

† Division of Medicinal Chemistry & Pharmacognosy, College of Pharmacy.

‡ Biophysics Program.

10.1021/ci900031y CCC: $40.75
Published on Web 05/18/2009

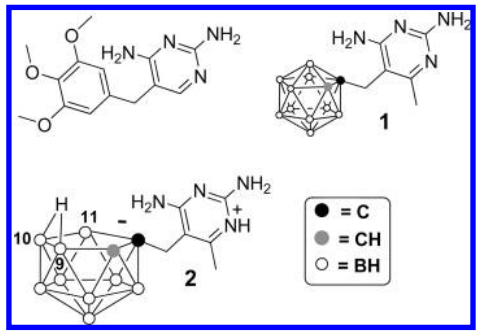

Figure 1. Trimethoprim and carboranyl antifolates **1** and **2**. The positioning of the "extra hydrogen" between B9−B10 corresponds to that in **2 N-crys** (see *Ligand Construction and Optimization* for further information).

METHODS

Docking Algorithms. AutoDock 4 is based on a Lamarckian genetic algorithm (LGA) method. Basically, this program determines total interaction energies between random pairs of ligands and various selected portions of protein to determine docking poses.[25,26] FlexX is a fragment based docking algorithm, which builds putative poses of the ligands using an incremental construction approach.[27−29] The modeling of protein−ligand interactions and their binding energy predictions is based on the *de novo* design tool LUDI.[28] Surflex generates putative poses for molecular fragments using a surface based molecular similarity method. This program employs the Hammerhead docking system for scoring.[30,31] Glide docking uses a series of hierarchical filters to find the best possible ligand binding locations in a prebuilt receptor grid space. The filters include a systematic search approach, which samples the positional, conformational, and orientational space of the ligand before evaluating the energy interactions of the ligand with the protein.[32,33]

Crystal Structures. PDB ID # 2C2S: human dihydrofolate reductase (hDHFR) complexed with [5-(1,2-*closo*-dicarbadodecarboran-1-yl)methyl]-2,4-diamino-6-methylpyrimidine (compound **1** in Figure 1)—this form of compound **1** will be referred to as **1 C-prot** throughout the paper. PDB ID # 2C2T: human DHFR complexed with a racemic mixture of [5-(7,8-*nido*-dicarbaundecarboran-7-yl)methyl]-2,4-diamino-6-methylpyrimidine (compound **2** in Figure 1)—this form of compound **2** will be referred to as **2 N-prot** throughout the paper.

Small molecule crystal structure data for **1** and **2** not complexed with hDHFR were generously provided by Dr. Steven Ealick, Cornell University, Ithaca, NY, and Dr. David Borhani, Harvard Medical School, Boston, MA.[10] These forms of **1** and **2** will be referred to as **1 C-crys** and **2 N-crys**, respectively, throughout the paper.

Ligand Construction and Optimization. 1 C-prot and both enantiomers of **2 N-prot** were extracted from their hDHFR crystal structures. The coordinates of the "extra hydrogen"[40] of **2 N-crys** were inserted into the structure of **2 N-prot**. Other hydrogen atoms were added to both **1 C-prot** and **2 N-prot** using the "add valence" option of GaussView. Mulliken-[34] and APT-[35] charges were calculated with Gaussian at the AM1-[36,37] and HF/6-31+G* levels.[38,39] ESPfit charges were calculated for **1 C-prot** and **2 N-prot** at the HF/6-31+G* level (Table 1). Compounds **1** and **2** were also constructed *de novo* without using crystallographic coordinates with HyperChem. These forms of **1** and **2** will be referred to as **1 C-con** and **2 N-con** throughout the paper. In the case of **2 N-con**, the *nido*-carboranyl moiety was aligned with the *closo*-carborane moiety of **1 C-prot**, and the coordinates for the "missing" boron atom were transferred and then changed to hydrogen. Optimization and Mulliken charge calculations for **1 C-con** and **2 N-con** were carried at the HF/6-31+G* level (Table 1). Following *de novo* construction and optimization of **2 N-con**, the "extra hydrogen" of the *nido*-cluster positioned itself between B10 and B11, while in the case of **2 N-crys**, the "extra hydrogen" was located between B9 and B10 (see Figure 1 and Supporting Information, Figure 1SI). In solution, the "extra hydrogen" appears to be in a fluxional equilibrium between B9/B10 and B10/B11.[40] Mulliken charges for **1 C-crys** and **2 N-crys** were calculated at the HF/6-31+G* level (Table 1).

Ligand Preparation. All Gaussian generated mol2 files of the ligands were aligned with the ligand coordinates of **1 C-prot** and **2 N-prot** using Sybyl before ligand preparation. AutoDock does not provide parameters that recognize boron atoms. Therefore, the boron atoms were changed to "C" by modifying the pdbqt (text) files. In the case of FlexX and Surflex, boron atoms were changed to "C.3" and "C", respectively. FlexX automatically converts boron atoms into "Du" (dummy) atoms if they are not changed to "C.3" by the user. Surflex does not have "Du" atom parameters, and it recognizes both boron and Du atoms as "funky atoms" and automatically changes their atom type to "C". Glide v 5. (OPLS2001) does not have boron and "Du" atom parameters. Therefore all the borons were replaced with "C.3".

AutoDock. All files generated for **1 C-prot**, **2 N-prot**, **1 C-crys**, **2 N-crys, 1 C-con**, and **2 N-con**, as described under 'Ligand Construction and Optimization', were used for docking. All nonpolar hydrogens were merged before saving the file into pdbqt format. Bonds of the carborane cages that were recognized as rotatable by AutoTors in ADT were changed to nonrotatable bonds. The total number of torsions (TORSDOF) for the written output files of all ligands was set to 2. FlexX: Only **1 C-crys**, **2 N-crys**, **1 C-con**, and **2 N-con** were used for docking (see Results and Discussion for details). FlexX automatically assigned formal charges on the ligands when they were imported into the FlexX environment. For docking in "user-defined" mode, either the 2,4-diamino-5-methyl pyrimidine portion (referred to as pyrimidyl portion [PP] throughout this manuscript), the 1,2-*closo*-dicarbadodecarboran-1-yl portion, or the 7,8-*nido*-dicarbaundecarboran-7-yl) portion was selected as a "base fragment". The latter two are referred to as carboranyl portions (CPs) throughout this manuscript. Surflex: Only **1 C-crys**, **2 N-crys**, **1 C-con**, and **2 N-con** were used for docking (see Results and Discussion for details). The input files generated for FlexX docking were also used for Surflex docking. As in the case of FlexX, Surflex operates with formal charges. For docking using the fragment placement method within the Surflex environment, PPs- or CPs were prepared from **2 N-crys** and **2 N-con** with HyperChem and imported into Surflex. Glide: **1 C-prot**, **2 N-prot**, **1 C-crys**, **2 N-crys, 1 C-con**, and **2 N-con**, as described under 'Ligand Construction and Optimization', were used for docking.

Protein Preparation. For docking with AutoDock, FlexX, and Surflex, the protein structures in pdb format were

Table 1. Optimization Characteristics and AutoDock Docking Patterns of Carboranyl Antifolates **1** and **2**

	AM1			HF/6-31+G*			
	Mulliken	APT	Mulliken	Mulliken	Mulliken	ESPfit	Mulliken
	1 C-prot	**1 C-prot**	**1 C-crys**	**1 C-prot**	**1 C-con**	**1 C-prot**	**1 C-crys**
BH[a]	0.079	−0.014	0.073	0.118	0.110	−0.0491	0.116
CH[b]	0.162	0.117	0.169	0.345	0.326	0.181	0.321
# of poses[c]	98	99	100	100	83	99	98
av binding energy[d] (kcal/mol)	−9.315	−4.697	−7.96	−3.895	−1.423	−4.984	−3.099
av RMSD[e]	0.581	0.575	0.86	0.530	0.666	0.5515	0.570
	2 N-prot[f]	**2 N-prot**[f]	**2 N-crys**[f]	**2 N-prot**[f]	**2 N-con**[f]	**2 N-prot**[f]	**2 N-crys**[f]
BH[a]	0.028	−0.099	0.038	0.058	0.056	−0.106	0.035
CH[b]	0.101	0.033	0.106	0.247	0.234	0.096	0.248
# of poses[c]	99	99	100	100	68	99	93
av binding energy (kcal/mol)[d]	−7.974	−4.337	−6.405	−2.164	−1.948	−2.195	−1.402
av RMSD[e]	0.629	0.631	0.543	0.741	0.499	0.603	0.574

[a] Average partial charge of all cage hydrogen atoms connected to boron. [b] Partial charge of cage hydrogen atom bound to carbon. [c] # of docked poses with RMSD below 2 Å (out of 100 docking solutions). [d] av binding energy for all the poses below 2 Å. [e] av RMSDs (Å) of all the poses below 2 Å. [f] The enantiomer of *nido*-carboranyl antifolates used for these calculations corresponds to the enantiomer of **2 N-prot** designated as 2B in the original crystal structure.[10]

prepared with the structure preparation tool of Sybyl. Monomers were separated from both crystal structures, and the blocking groups AMI and CXC were added to the N- and C-terminis, respectively, for neutralization. Water molecules were removed, hydrogen atoms were added, and side chain amides and side chains bumps were fixed. In the case of AutoDock, pdb files along with the NADPH (nicotinamide adenine dinucleotide phosphate) cofactor were imported into the ADT environment, atom types were assigned, and Gasteiger charges were added. For FlexX, the NADPH cofactor was removed from the pdb files and saved as a separate mol2 file before defining the active site. The receptor description files (rdf) for docking were created with Sybyl using both hDHFR crystal structures. The amino acids within a 6.5 Å radius of **1 C-prot** and **2 N-prot** were selected to define the active site. The pdb, rdf, and NADPH mol2 files were then imported into the FlexX environment. For Surflex, pdb files containing NADPH were imported into the Surflex environment. Protomol files[30,31] were generated using **1 C/2 N-crys** and **1 C/2 N-con** separately.

In the case of Glide, protein coordinates were preprocessed for docking using the Protein Preparation Wizard provided in the Schrodinger Maestro environment. Hydrogen atoms were added, and the bond orders were assigned after deleting the monomer B as well as water molecules. Assignment of protonation states was carried out followed by hydrogen bond optimization for hydroxyl groups as well as Asn, Gln, and His residues. The hydrogen atoms were then minimized with the OPLS2001 force field. Grid calculations were performed for the protein residues of the active sites with **1 C-prot** and **2 N-prot** coordinates as the center with default box size (grid box center x,y,z coordinates = 2.285766, 29.832586, −3.303069; grid box cube size in x,y,z direction = 21.816994 Å).

Docking. AutoDock. The Lamarckian genetic algorithm (LGA) was selected for the ligand conformational search. The docking area was defined using AutoGrid 4. A 40 × 40 × 40 3-D affinity grid centered around the antifolate binding site with a 0.375 Å grid point spacing was calculated for each of the following atom types: (a) protein: A (aromatic C), C, HD, N, NA, OA, SA and (b) ligand: C, A, HD, N, NA, e (electrostatic), and d (desolvation). Additional docking parameters were: Dockings trials: 100, population size: 100, random starting position and conformation, translation step ranges: 2.0 Å, rotation step ranges: 50, elitism: 1, mutation rate: 0.02, crossover rate: 0.8, local search rate: 0.06, and energy evaluations: 250,000. Higher energy evaluations (2,500,000) or higher population sizes (250) did not alter docking performances significantly. Final docked conformations were clustered using a tolerance of 2 Å root-mean-square deviations (RMSD). FlexX: Docking was performed in command line mode. The cofactor NADPH was read using a separate mol2 file as a part of the active site. Docking in the automated mode proceeded with an automated base fragment selection, which is followed by placement algorithm 3 (PA3). User-defined base fragment selection was followed by PAs 1, 2, or 3[27,29] and incremental build up of the entire ligand. Surflex: Default-, multistart 5-, and fragment placement (only **2 N-crys** and **2 N-con)** modes were explored. Glide: Final calculations were performed with the Standard-Precision (SP) rigid docking protocol. Ten thousand poses were kept in the initial phase of the docking keeping the default scoring window cutoff level 100. Ligand van der Waals radii were scaled to a factor of 0.80 for nonpolar atoms with a partial charge cutoff level of 0.15 (absolute value). A maximum of 100 conformations with the best binding energies was retained for the final analysis while discarding poses with less than 0.01 Å RMSD and 0.01 Å atomic displacement as duplicates.

Docking Comparisons. As stated above, the four docking programs are based on different algorithms, and it may be difficult to directly compare the results obtained with each of the programs, as has been discussed previously by Cole et al.[41] Apart from AutoDock, the other docking programs did not generate large numbers of duplicate poses within a RMSD of 2 Å. Therefore, a comparison of the av RMSDs of all docked poses would be meaningless for FlexX, Surflex, and Glide. However, in the case of the latter three programs, approximately the top 25% of all docked poses (based on the binding energies) were below 4 Å of RMSD. In addition, the top ranked poses accurately reproduced the binding mode of the ligands in the crystal structure. Therefore, we used

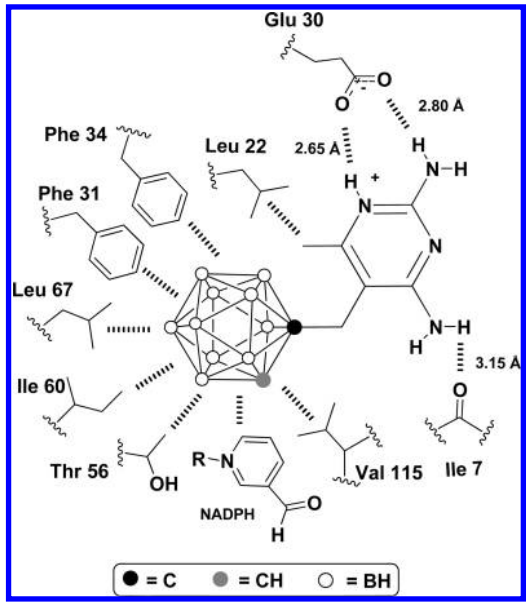

Figure 2. Binding of **1C-prot** with various active site amino acid residues of hDHFR. The **2N-prot** enantiomers have similar binding interactions in the hDHFR active site.[10]

the top 25% of the poses and the top ranked poses to compare the docking results from FlexX, Surflex, and Glide.

Scoring. AutoDock, FlexX, and Glide predict the free energy of binding in terms of kcal/mol.[25,28,31] Surflex predicts the binding affinity of the ligand-protein complex in the form of $-\log(K_d)$.[42] In order to compare scoring features appropriately, the Surflex scoring values were converted into free energy of binding values using the following equation: kcal/mol $= 0.59 \log_e (10^{-pK_d})$.[42]

RESULTS AND DISCUSSION

The binding interactions of **1 C-prot** and both enantiomers of **2 N-prot** with amino acid residues in the original hDHFR crystal structures have been discussed previously by Reynolds et al.[10] **1 C-prot** and **2 N-prot** showed almost identical binding poses in the hDHFR crystal structures, as shown in Figure 3A. The additional BH vertex of the *closo*-cage of **1 C-prot** is positioned slightly above the center of the open faces of the *nido*-cages of **2 N-prot.** This binding pattern is similar to that of trimethoprim in the active site of hDHFR. The carborane cages of **1 C-prot** and **2 N-prot** bind to the same hydrophobic pocket of hDHFR as the trimethoxyphenyl group of trimethoprim. The 2,4-diamino-5-methylpyrimidine moieties of **1 C-prot** and **2 N-prot** form hydrogen bonds with various amino acid residues in the active site (Glu 30, Ile 7, Val 115), as shown in Figure 2 using the example of **1 C-prot**. The binding between amino acid residues of the active site with both the neutral *closo*-cage of **1 C-prot** and the presumably negatively charged *nido*-cages of **2 N-prot** are typical for hydrophobic interactions. Similar hydrophobic interactions were observed for a metallocarborane, consisting of two negatively charged *nido*-carboranes, bound to HIV protease.[13] Proton-hydride type bonds[43,44] may not play major roles in the interactions of the carboranyl moieties of **1 C-prot** and **2 N-prot** with active site amino acid residues, as is evident from the orientations of the Thr56 hydroxyl groups in the original hDHFR crystal structures, which point away from the cages (see also Figure 2).

An analysis of the docking studies with **1 C-crys**, **2 N-crys**, **1 C-prot, 2 N-prot, 1 C-con,** and **2 N-con** using AutoDock is shown in Table 1 and Figure 3B,C. The number of docked poses for the *closo*-carboranyl structures with a RMSD below 2 Å was in all cases high (83−100) with minimal differences in av RMSDs (0.53 Å− 0.86 Å). With the exception of **1 C-con**, the *nido*-carboranyl structures showed similar docking patterns with 93−100 poses having an RMSD below 2 Å and av RMSDs between 0.5 and 0.74 Å. In the case of **2 N-con**, 68% of the docked poses had RMSDs lower than 2 Å, while 32% had an av RMSD of 5.2 Å. A detailed analysis of this minor cluster revealed that the pose of the *nido-o*-carboranyl portion did not show any significant deviation from its counterpart in the original crystal structure, while the pose of the 2,4-diaminopyrimidyl portion was altered forming a strong hydrogen bond with Asp 21 rather than with Glu 30, as in the case of crystallized ligand (Figure 3D). In the case of **2 N-con**, the *de novo* construction and optimization resulted in a different location of the "extra hydrogen" compared with **2 N-crys** and **2 N-prot** (see Figure 1 and Supporting Information, Figure 1SI), which may have contributed to the occurrence of the minor cluster. In general, both enantiomers of **2** showed similar docking patterns (data not shown).

The boron-bound hydrogen atoms (1−6, 9−11) (see Figure 1 and Supporting Information, Figure 1SI) in carboranes are predicted to be slightly more electronegative than carbon-bound hydrogen[42,43] and may have on average negative partial charges. According to ESPfit calculations, the average partial charges for these hydrogens are about −0.24 for 2-fold negatively charged *nido*-carborane $[C_2B_9H_{11}]^{2-}$, −0.15 for 1-fold negatively charged *nido*-carborane $[C_2B_9H_{12}]^{-}$, and −0.07 for neutral *nido*-carborane $[C_2B_9H_{13}]$.[43,44] The charges generated in our own ESPfit calculations for **1 C-prot** and **2 N-prot** (Table 1) are consistent with those reported in the literature.[43,44] However, Mulliken charges obtained for **1 C-prot** and **2 N-prot** were generally more positive.

Overall, the docking results obtained with AutoDock indicate that minor differences in geometries, stemming from different data sources and/or optimization methods/calculations (e.g., "extra hydrogen" position), and partial atomic charges did not have a major impact on docking accuracy although they seemed to affect the av binding energies to some extent (Table 1). In general the binding energies were somewhat lower for the *nido*-carboranyl antifolates compared with their *closo*-carboranyl counterparts.

In an attempt to further validate our strategy to enable docking of biomolecules containing boron clusters by replacing boron with carbon, we tried to implement known boron parameters into AutoDock before docking. Borons atoms in cage structures, such as *closo-o*-carborane and *nido*-carboranes, are hexavalent. To the best of our knowledge, no force field parameters for this boron atom type are available. So far only MM2 force field parameters for sp3 boron, as in borates, have been described.[20,45] These parameters include nonbonded interaction of sp3 borons, such as the van der Waals energy well depth and the van der Waals radius. Information related to the atomic solvation parameter for sp3 borons is not available. Therefore, only partial implementation of sp3 boron parameters into AutoDock has been carried out. With respect to values related to atomic solvation and

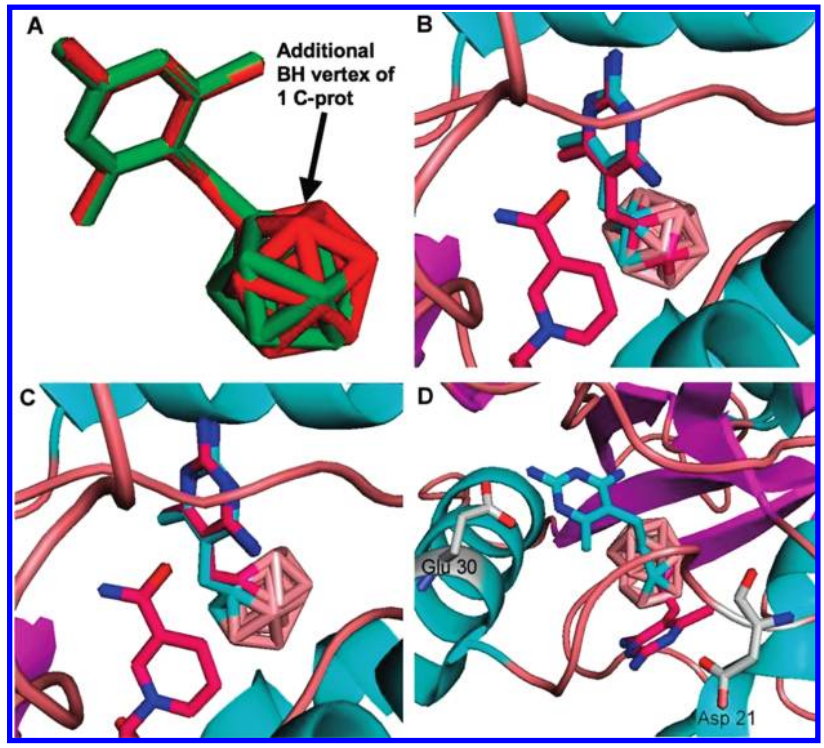

Figure 3. (A) Overlap of the crystal structures poses of **1C-prot** (red) and **2 N-prot** (green).[10] (B) Overlap of the docked pose (AutoDock) of **1C-con** (magenta) with the corresponding pose of **1C-prot** (cyan) in the original crystal structure (av RMSD: 0.666 Å). (C) Overlap of the docked pose (AutoDock, major cluster with 68 solutions) of **2 N-con** (magenta) with the corresponding pose of **2 N-prot** (cyan) in the original crystal structure (av RMSD: 0.499 Å). (D) Overlap of the docked pose (AutoDock) of **2 N-con** (magenta) with the corresponding pose of **2 N-prot** (cyan) in the original crystal structure. The av RMSD of the minor cluster (32 poses) is 5.22 Å.

other parameters, the corresponding carbon atom type parameters were used (see the Supporting Information). Overall, the docking patterns for **1 C/2 N-crys**, **1 C/2 N-prot**, and **1 C/2 N-con** following partial implementation of sp3 boron parameter were found to be comparable to those using exclusively carbon parameters (see Table 1SI in the Supporting Information for details).

The Glide docking program uses ConfGen, a systematic sampling method to generate several conformations of the ligand prior to the actual docking calculation. Initially, the switch of boron atom type to "C.3" atom type using the ConfGen failed to generate conformations of the ligands because the atomic bonds in the cage structures of the ligands were considered as torsions. Therefore, we adopted a rigid docking protocol, which did not directly use the conformational sampling capability in Glide. The docking results for **1 C-crys** and **2 N-crys** using this approach are shown in Table 2. Overall, Glide reproduced the crystal binding modes closely as can be seen by the av RMSDs of the top 25% poses. The av binding energy of the top 25% poses was also very close to the binding energy of the top ranked pose.

The impact of charge differences on the carborane clusters as a result of different data sources and/or optimization methods/calculations was also explored with Glide (see Supporting Information, Table 2SI). As in the case of AutoDock docking, the binding energies were lower for the *nido*-carboranyl antifolates compared to the *closo*-carboranyl counterparts. Overall, differences in av binding energies, as a result of different geometries and partial atom charges, were not as pronounced as in the case of AutoDock, while RMSDs and pose clustering were comparable.

Since FlexX and Surflex operate with formal charges,[27,28,30,31] only docking of **1 C/2 N-crys** and **1 C/2 N-con** was evaluated with these programs. The latter carboranyl antifolates were chosen to address the influence of geometric differences on the docking performances. Automated docking of **1 C-crys** and **2 N-crys** by FlexX produced top ranked poses with RMSDs of 3.19 Å and 3.18 Å, respectively. The top 25% of the docked poses for both **1 C-crys** and **2 N-crys** had av RMSDs of 5.97 Å and 5.89 Å, respectively (Tables 3 and 4). The automated mode selected the PPs of **1 C-crys** and **2 N-crys** as the base fragments and PA3 before incremental construction of the ligands. User defined base fragment placement (BFP) of the PP of **1 C-crys** followed by PA1 and PA2 improved the RMSDs of the top-ranking poses by factors of 1.6 and 2, respectively, and the av RMSDs of top 25% poses by factors of 3.2 and 1.4, respectively. The corresponding improvement factors in the case **2 N-crys** were 2.5, 1.6, 1.7, and 1.0. As expected, user defined BFP of PP, followed by PA3, produced the same results as automated docking. **1 C-con**

Table 2. Glide Docking of **1 C-crys** and **2 N-crys**

parameters	**1 C-crys**[c]	**2 N-crys**[c]
RMSD of the top ranked pose (Å)[a]	0.13	0.30
binding energy of the top ranked pose (kcal/mol)	−9.40	−7.90
av RMSD of the top 25% poses (Å)[b]	0.11	0.29
av binding energy of the top 25% poses (kcal/mol)	−9.27	−7.80
no. of docking solutions	100	100

[a] Pose with the lowest binding energy. [b] Top 25% poses according to binding energies. [c] Mullican charges obtained at the HF/6-31+G* level were used for docking of **1 C-crys** and **2 N-crys** (see Table 1).

Table 3. Effects of Automated Docking Mode, Selection of Base Fragment for Placement (BFP), and Placement Algorithm (PA) on FlexX Docking of **1 C-crys and 2 N-crys**

		user defined docking				
		PP[a]			CP[b]	
	automated docking	PA1[c]	PA2[d]	PA3[e]	PA2[c]	PA3[e]
1 C-crys						
RMSD of the top ranked pose (Å)[f]	3.19	2.01	1.62	3.19	6.44	2.38
binding energy of the top ranked pose (kcal/mol)	−10.73	−25.64	−23.27	−10.73	−9.93	−17.06
av RMSD of the top 25% poses (Å)[g]	5.97	1.84	4.15	5.97	3.95	3.66
av binding energy of the top 25% poses (kcal/mol)	−7.18	−21.10	−12.87	−7.18	−8.46	−5.28
pose with the lowest RMSD (Å) and its energy rank	3.19 (1)	0.96 (7)	1.41 (2)	3.19 (1)	2.19 (5)	1.39 (3)
total no. of docking solutions	41	41	77	41	29	54
2 N-crys						
RMSD of the top ranked pose (Å)[f]	3.18	1.27	2.00	3.18	6.25	6.47
binding energy of the top ranked pose (kcal/mol)	−13.67	−16.23	−20.33	−13.67	−8.32	−9.90
av RMSD of the top 25% poses (Å)[g]	5.89	3.50	5.5	5.89	6.24	5.34
av binding energy of the top 25% poses (kcal/mol)	−9.82	−15.44	−12.05	−9.82	−5.85	−6.26
pose with the lowest RMSD (Å) and its energy rank	3.18 (1)	1.24 (5)	0.82 (3)	3.18 (1)	3.33 (15)	3.01 (19)
total no. of docking solutions	28	26	74	28	40	53

[a] Docking using the pyrimidyl portion (PP) for base fragment placement (BFP). [b] Docking using the *closo-o*-carboranyl portion (CP) for BFP. [c] Placement algorithm 1 (PA1). [d] Placement algorithm 2 (PA2). [e] Placement algorithm 3 (PA3). [f] Top ranking pose according to binding energies. [g] Top 25% poses according to binding energies. PA1 did not result in docking solutions for **1 C-crys** and **2 N-crys** when **CP** was chosen as BFP.

Table 4. Surflex Docking of **1 C-crys** and **2 N-crys**

	1 C-crys		**2 N-crys**		**2 N-crys**	
parameters	default settings	multistart 5[c]	default settings	multistart 5[c]	PP placement and multistart 5[c]	CP placement and multistart 5[c]
RMSD of the top ranked pose (Å)[a]	0.883	1.998	0.741	0.755	0.671	0.463
binding energy of the top ranked pose[a] (kcal/mol)	−9.74	−9.93	−7.12	−7.16	−7.16	−7.24
av RMSD of the top 25% poses (Å)[b]	0.78	1.41	3.25	1.97	0.731	1.26
av total binding energy of the 25% poses[b] (kcal/mol)	−9.58	−9.78	−7.06	−7.13	−7.11	−7.19
pose with lowest RMSD (Å) and its energy rank indicated in bracket	0.448 (4)	0.448 (15)	0.646 (6)	0.573 (2)	0.671 (1)	0.463 (1)
no. of docking solutions	20	20	20	20	20	20

[a] Pose with the lowest binding energy. [b] Top 25% poses with the lowest binding energy. [c] Docking with 5 different starting positions; PP: Pyrimidyl Portion; CP: Carboranyl Portion.

and **2 N-con** produced similar FlexX docking results indicating that in the absence of crystal structure information, binding interactions of virtual carboranyl compounds with proteins can be predicted accurately (see Supporting Information, Table 3SI).

For BFP, both in automated and user defined mode, FlexX favors PP. User defined BFP of CPs, in particular in the cases of **2 N-crys** and **1 C/2 N-con**, was inferior to BFP of PP indicating that hydrogen bonds and/or ionic interactions may be favored in this initial phase of the FlexX docking.[27,28] This may also explain the fact that user defined BFP of CPs, produced poor docking solutions with high RMSDs. PA1 was found to be superior to PA2 and PA3 following initial BFP of PP. PA1 only utilizes interactions that are hydrophobic and unspecific in nature.[27] This indicates that the second phase of incremental construction in FlexX docking, involving the PAs, is mainly guided by the hydrophobicity of the CPs.

The results of Surflex docking of **1 C-crys** and **2 N-crys** are summarized in Table 4. Using default docking parameters without fragment placement, the top 25% poses of **1 C-crys** have an av RMSD of 0.78 Å and the top ranking pose had an RMSD of 0.89 Å. Docking of **1 C-crys** using the "multistart5" option (5 different starting positions) without fragment placement decreased the docking quality of both top 25% poses and top ranked pose by a factor ∼ 2. Docking with fragment placement was not explored because the default settings produced satisfactory docking results. In the case **1 C-con**, there were no significant differences in docking quality between default settings and the "-multistart5" option (see Supporting Information, Table 4SI).

Docking of **2 N-crys** using default parameters without fragment placement was unsatisfactory resulting in an av RMSD of the top 25% poses of 3.25 Å. The "multistart5" option without fragment placement improved the docking by a factor of 1.65 (1.97 Å). The difference in RMSDs of the top ranked poses was insignificant (0.741 vs 0.755 Å). These values improved even further for docking with fragment placement. When PP was selected as a placed fragment, the corresponding av RMSD and the top ranking pose RMSD decreased to 0.731 and 0.671 Å, respectively. The corresponding values for fragment placement of CPs

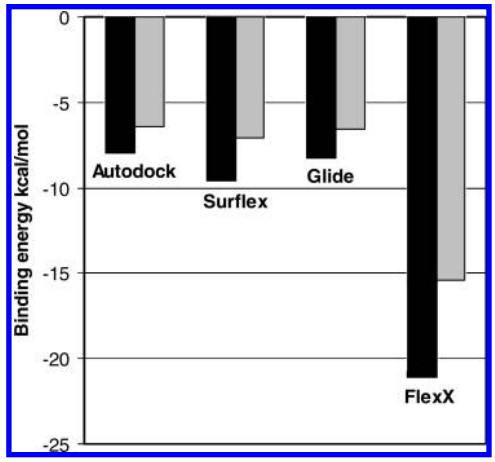

Figure 4. Average total binding energies of docked **1 C-crys** (black bar) and **2 N-crys** (gray bar) with hDHFR. For AutoDock and Glide, Mulliken charges at the AM1 level were considered for **1C-crys** and **2 N-crys**. For Surflex, FlexX, and Glide, the av binding energies for the top 25% poses were considered. For AutoDock, the av binding energies of all poses were considered.

were 1.26 Å and 0.463 Å. This is in contrast to FlexX, where BFP of the *nido*-CP led to a significant deterioration of docking quality. Overall, the Surflex docking results for **2 N-con** showed similar patterns as for those of **2 N-crys** (see Supporting Information, Table 4SI).

In preliminary studies, we also explored the Molecular Operating Environment (MOE) program for docking of carboranyl antifolates into hDHFR. Docking was carried out in standard mode. MOE is based on simulated annealing, which calculates the grid based interaction energy between the docked ligand and the receptor/enzyme.[46,47] MOE has parameter sets for sp2 and sp3 boron atoms but not for hexavalent boron. If at all, the docking performance of MOE seemed to be comparable with that of FlexX in automated mode. Both replacement of boron with "C.3" and the use of the boron atom types provided by MOE produced similar docking results.

Enzymatic studies indicated that antifolate **1** is approximately ten times more potent than **2** as an inhibitor of hDHFR,[10] which is consistent with the binding energies that were predicted by all four docking programs for **1** and **2** (Figure 4). However, these free energy values should be viewed with caution. Scoring functions are in general not very accurate with significant differences between various docking algorithms.[48] Additionally, the hydrophobic interactions were calculated without applying appropriate force fields for hexavalent boron.

SUMMARY AND CONCLUSIONS

This is the first report of docking studies with compounds containing the negatively charged *nido*-carboranyl cluster. Using **1 C-crys** and **2 N-crys** as examples, the docking performances of AutoDock, Glide, FlexX, and Surflex are summarized in Figure 5. Under optimized conditions (e.g., rigid docking and fragment placements), docking of **1 C-crys** with AutoDock and Glide was comparably good followed by Surflex and then FlexX. In the case of **2 N-crys**, AutoDock, Glide, and Surflex showed comparably good docking followed by FlexX. Under optimized conditions, docking of **1 C-crys** and **2 N-crys** is comparable when

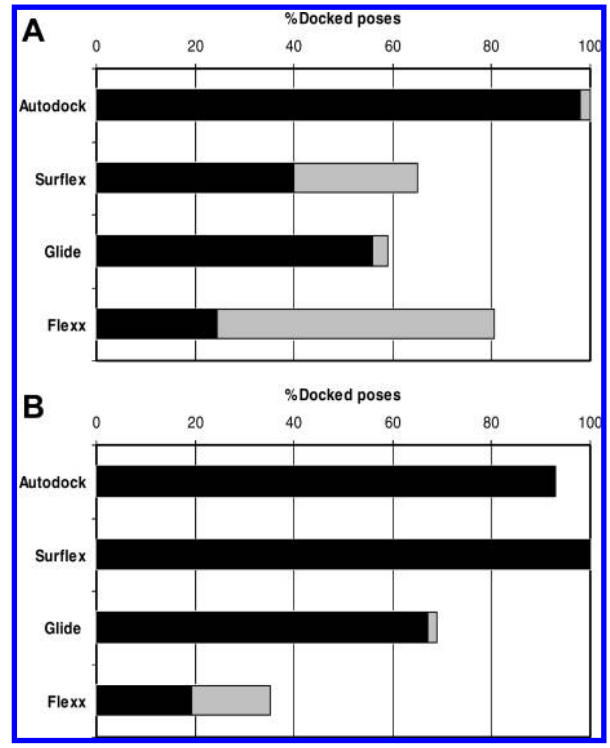

Figure 5. Comparative docking evaluation of **1 C-crys (A)** and **2 N-crys (B)**. The black bars indicate the percentage of the total poses with RMSD below 2 Å, and the gray bars indicate the percentage of the total poses with RMSDs below 4 Å. Data used for this presentation are based on Mulliken charges obtained at the HF/6-31+G* level for AutoDock and Glide, rigid docking mode for Glide, and BFP of PP with PA1 for FlexX. For Surflex docking, default settings without fragment placement were used for **1 C-crys** and PP placement combined with multistart 5 option for **2 N-crys**.

AutoDock, Glide, and FlexX were used. In the case of Surflex, however, **2 N-crys** docked better than **1 C-crys**. Overall, a comparative evaluation of **1 C-con** and **2 N-con** produced similar results (Supporting Information, Figure 2SI).

Differences in geometries and partial atom charges resulting from different data sources and/or optimization methods/calculations did not impact the docking performances of AutoDock and Glide significantly. A careful selection of placement algorithm and/or fragment placement improved the docking quality of both FlexX and Surflex. The scoring values generated by all four programs were in accordance with experimental data. The observed docking patterns of *closo*- and *nido*-carboranyl antifolates with hDHFR validate previously developed methods for structure and ligand-based design of carborane-containing compounds.[16,49]

The force field parameters developed for sp3 borons by Otkidach et al.[20,45] were partially implemented in AutoDock for docking of the carboranyl antifolates. The described docking model appears to remain unaffected by this substitution, which further validates our strategy to enable docking of biomolecules containing boron clusters by replacing boron with carbon. It should be noted, however, that apart from AutoDock the implementation of these parameters in the other softwares packages discussed in the present study is not straightforward.

Carborane cages are rigid, hydrophobic entities, and, intuitively, the docking of these scaffolds could be visualized as the docking of a single hydrophobic entity into the hydrophobic

pocket of hDHFR. From this perspective, it is difficult to envision how the interactions of this single entity with its amino acid environment are changed during the docking process by replacing hexavalent boron either with carbon or sp3 boron. Although the reported docking protocols could be validated successfully, there is certainly further need for the development of accurate forcefield parameters, probably for the entire cage structures rather than for individual atom types.

A drawback of the present study was that the carboranyl antifolates used for docking only contained two rotatable bonds at the methylene bridge between the carboranyl- and the pyrimidyl portions. Consequently, the torsional degrees of freedom were limited in the present study, and evaluating more complex systems may be necessary to confirm that the reported docking protocols are also applicable to other biomolecules that contain carborane clusters. Unfortunately, such systems are currently not available.

Abbreviations. 1 C-prot, *closo-o*-carboranyl antifolate (**1**) cocrystallized with hDHFR (PDB # 2C2S); **2 N-prot**, *nido-o*-carboranyl antifolate (**2**) cocrystallized with the hDHFR (PDB # 2C2T); **1 C-crys**, small molecule crystal structure of the *closo-o*-carboranyl antifolate (**1**); **2 N-crys**, small molecule crystal structure of the *nido-o*-carboranyl antifolate (**2**); **1 C-con**, *de novo* constructed form of *closo-o*-carboranyl antifolate (**1**); **2 N-con**, *de novo* constructed form of the *nido-o*-carboranyl antifolate (**2**); ADT, AutoDock Tools; APT, Atomic Polar Tensors; Av, Average; BFP, Base Fragment Placement; ESPfit, Electrostatic Potential Fit Method; BNCT, Boron Neutron Capture Therapy; Du, Dummy atom type; hDHFR, human Dihydrofolate Reductase; LGA, Lamarckian Genetic Algorithm; MOE, Molecular Operating Environment; NADPH, Dihydronicotinamide Adenine Dinucleotide Phosphate; PA1, Placement Algorithm 1; PA2, Placement Algorithm 2; PA3, Placement Algorithm 3; PP, pyrimidyl portion used as a base fragment; CP, *closo-o*-carboranyl- or *nido-o*-carboranyl portion used as a base fragment; rdf, receptor description file; RMSD, Root Mean Square Deviation; SP, Standard Precision.

ACKNOWLEDGMENT

The presented work was financially supported by funds from The Ohio State University College of Pharmacy and, in part, by NIH grant 1 R01 CA127935-01A2. The authors would like to thank Drs. Steven Ealick for generously providing the small molecule crystal structure parameters of **1** and **2**. Dr. David Borhani and Dr. Richard Dixon (Abbott Bioresearch Centre, Worcester, MA), Dr. Holger Claussen (BioSolveIT), Dr. Christopher Williams (Chemical Computing Group), and Dr. Jeffrey Saunders (Schrodinger, LLC) are acknowledged for helpful discussions. The authors of this manuscript are grateful to In Hee Park for her help with implementation of boron parameters in AutoDock Tools. This paper was presented in part at the European Science Foundation (ESF) Exploratory Workshop "BioBor-Exploring New Opportunities of Boron Chemistry Towards Medicine", in Lodz, Poland, May 9−12, 2008.

Supporting Information Available: This material is available free of charge via the Internet at http://pubs.acs.org.

REFERENCES AND NOTES

(1) Armstrong, A. F.; Valliant, J. F. The bioinorganic and medicinal chemistry of carboranes: from new drug discovery to molecular imaging and therapy. *Dalton Trans.* **2007**, *38*, 4240–4251.
(2) Lesnikowski, Z. J. Boron units as pharmacophores - new applications and opportunities of boron cluster chemistry. *Collect. Czech. Chem. Commun.* **2007**, *72*, 1646–1658.
(3) Endo, Y.; Iijima, T.; Yaguchi, K.; Kawachi, E.; Inoue, N.; Kagechika, H.; Kubo, A.; Itai, A. Structure-Activity study of retinoid agonists bearing substituted dicarba-closo-dodecaborane. Relation between retinoidal activity and conformation of two aromatic nuclei. *Bioorg. Med. Chem. Lett.* **2001**, *11*, 1307–1311.
(4) Ogawa, T.; Ohta, K.; Yoshimi, T.; Yamazaki, H.; Suzuki, T.; Ohta, S.; Endo, Y. *m*-Carborane bisphenol structure as a pharmacophore for selective estrogen receptor modulators. *Bioorg. Med. Chem. Lett.* **2006**, *16*, 3943–3946.
(5) Goto, T.; Ohta, K.; Suzuki, T.; Ohta, S.; Endo, Y. Design and synthesis of novel androgen receptor antagonists with sterically bulky icosahedral carboranes. *Bioorg. Med. Chem.* **2005**, *13*, 6414–6424.
(6) Endo, Y.; Yoshimi, T.; Kimura, K.; Itai, A. Protein kinase C modulators bearing dicarba-closo-dodecaborane as a hydrophobic pharmacophore. *Bioorg. Med. Chem. Lett.* **1999**, *9*, 2561–2564.
(7) Tsuji, M.; Koiso, Y.; Takahashi, H.; Hashimoto, Y.; Endo, Y. Modulators of tumor necrosis factor alpha production bearing dicarba-closo-dodecaborane as a hydrophobic pharmacophore. *Biol. Pharm. Bull.* **2000**, *23*, 513–516.
(8) Julius, R. L.; Farha, O. K.; Chiang, J.; Perry, L. J.; Hawthorne, M. F. Synthesis and evaluation of transthyretin amyloidosis inhibitors containing carborane pharmacophores. *Proc. Natl. Acad. Sci. U. S. A.* **2007**, *104*, 4808–4813.
(9) Page, M. F. Z.; Jalisatgi, S. S.; Maderna, A.; Hawthorne, M. F. Design and synthesis of a candidate alpha -human thrombin irreversible inhibitor containing a hydrophobic carborane pharmacophore. *Synthesis* **2008**, *4*, 555–563.
(10) Reynolds, R. C.; Campbell, S. R.; Fairchild, R. G.; Kisliuk, R. L.; Micca, P. L.; Queener, S. F.; Riordan, J. M.; Sedwick, W. D.; Waud, W. R.; Leung, A. K. W.; Dixon, R. W.; Suling, W. J.; Borhani, D. W. Novel boron-containing, nonclassical antifolates: Synthesis and preliminary biological and structural evaluation. *J. Med. Chem.* **2007**, *50*, 3283–3289.
(11) Tolmachev, V.; Koziorowski, J.; Sivaev, I.; Lundqvist, H.; Carlsson, J.; Orlova, A.; Gedda, L.; Olsson, P.; Sjoeberg, S.; Sundin, A. Closo-Dodecaborate(2-) as a Linker for Iodination of Macromolecules. Aspects on Conjugation Chemistry and Biodistribution. *Bioconjugate Chem.* **1999**, *10*, 338–345.
(12) Wilbur, D. S.; Chyan, M.-K.; Hamlin, D. K.; Vessella, R. L.; Wedge, T. J.; Hawthorne, M. F. Reagents for astatination of biomolecules. 2. Conjugation of anionic boron cage pendant groups to a protein provides a method for direct labeling that is stable to in vivo deastatination. *Bioconjugate Chem.* **2007**, *18*, 1226–1240.
(13) Kozisek, M.; Cigler, P.; Lepsik, M.; Fanfrlik, J.; Rezacova, P.; Brynda, J.; Pokorna, J.; Plesek, J.; Gruner, B.; Grantz Saskova, K.; Vaclavikova, J.; Kral, V.; Konvalinka, J. Inorganic polyhedral metallacarborane inhibitors of HIV protease: A new approach to overcoming antiviral resistance. *J. Med. Chem.* **2008**, *51*, 4839–4843.
(14) Moore, B. S.; Eustaquio, A. S.; McGlinchey, R. P. Advances in and applications of proteasome inhibitors. *Curr. Opin. Chem. Biol.* **2008**, *12*, 434–440.
(15) Hawthorne, M. F.; Lee Mark, W. A critical assessment of boron target compounds for boron neutron capture therapy. *J Neurooncol.* **2003**, *62*, 33–45.
(16) Bandyopadhyaya, A. K.; Tiwari, R.; Tjarks, W. Comparative molecular field analysis and comparative molecular similarity indices analysis of boron-containing human thymidine kinase 1 substrates. *Bioorg. Med. Chem.* **2006**, *14*, 6924–6932.
(17) Johnsamuel, J.; Byun, Y.; Jones, T. P.; Endo, Y.; Tjarks, W. A new strategy for molecular modeling and receptor-based design of carborane containing compounds. *J. Organomet. Chem.* **2003**, *680*, 223–231.
(18) Martichonok, V.; Jones, J. B. Cysteine proteases such as papain are not inhibited by substrate analog peptidyl boronic acids. *Bioorg. Med. Chem.* **1997**, *5*, 679–684.
(19) Minkkila, A.; Saario, S. M.; Kasnanen, H.; Leppanen, J.; Poso, A.; Nevalainen, T. Discovery of boronic acids as novel and potent inhibitors of fatty acid amide hydrolase. *J. Med. Chem.* **2008**, *51*, 7057–7060.
(20) Tafi, A.; Agamennone, M.; Tortorella, P.; Alcaro, S.; Gallina, C.; Botta, M. AMBER force field implementation of the boronate function to simulate the inhibition of beta -lactamases by alkyl and aryl boronic acids. *Eur. J. Med. Chem.* **2005**, *40*, 1134–1142.
(21) Byun, Y.; Thirumamagal, B. T. S.; Yang, W.; Eriksson, S.; Barth, R. F.; Tjarks, W. Preparation and biological evaluation of 10B-

Enriched 3-[5-{2-(2,3-Dihydroxyprop-1-yl)-o-carboran-1-yl}pentan-1-yl]thymidine (N5−2OH), a new boron delivery agent for boron neutron capture therapy of brain tumors. *J. Med. Chem.* **2006**, *49*, 5513–5523.

(22) Narayanasamy, S.; Thirumamagal, B. T.; Johnsamuel, J.; Byun, Y.; Al-Madhoun, A. S.; Usova, E.; Cosquer, G. Y.; Yan, J.; Bandyopadhyaya, A. K.; Tiwari, R.; Eriksson, S.; Tjarks, W. Hydrophilically enhanced 3-carboranyl thymidine analogues (3CTAs) for boron neutron capture therapy (BNCT) of cancer. *Bioorg. Med. Chem.* **2006**, *14*, 6886–6899.

(23) Chazalette, C.; Riviere-Baudet, M.; Scozzafava, A.; Abbate, F.; Maarouf, Z. B.; Supuran, C. T. Carbonic anhydrase inhibitors, interaction of boron derivatives with isozymes I and II: a new binding site for hydrophobic inhibitors at the entrance of the active site as shown by docking studies. *J. Enzyme Inhib.* **2001**, *16*, 125–133.

(24) Endo, Y.; Iijima, T.; Yamakoshi, Y.; Fukasawa, H.; Miyaura, C.; Inada, M.; Kubo, A.; Itai, A. Potent estrogen agonists based on carborane as a hydrophobic skeletal structure: a new medicinal application of boron clusters. *Chem. Biol.* **2001**, *8*, 341–355.

(25) Huey, R.; Morris, G. M.; Olson, A. J.; Goodsell, D. S. A semiempirical free energy force field with charge-based desolvation. *J. Comput. Chem.* **2007**, *28*, 1145–1152.

(26) Morris, G. M.; Goodsell, D. S.; Halliday, R. S.; Huey, R.; Hart, W. E.; Belew, R. K.; Olson, A. J. Automated docking using a lamarckian genetic algorithm and an empirical binding free energy function. *J. Comput. Chem.* **1998**, *19*, 1639–1662.

(27) Rarey, M.; Kramer, B.; Lengauer, T. Docking of hydrophobic ligands with interaction-based matching algorithms. *Bioinformatics* **1999**, *15*, 243–250.

(28) Rarey, M.; Kramer, B.; Lengauer, T.; Klebe, G. A fast flexible docking method using an incremental construction algorithm. *J. Mol. Biol.* **1996**, *261*, 470–489.

(29) Rarey, M.; Wefing, S.; Lengauer, T. Placement of medium-sized molecular fragments into active sites of proteins. *J. Comput.-Aided Mol. Des.* **1996**, *10*, 41–54.

(30) Jain, A. N. Surflex: fully automatic flexible molecular docking using a molecular similarity-based search engine. *J. Med. Chem.* **2003**, *46*, 499–511.

(31) Jain, A. N. Surflex-Dock 2.1: Robust performance from ligand energetic modeling, ring flexibility, and knowledge-based search. *J. Comput.-Aided Mol. Des.* **2007**, *21*, 281–306.

(32) Friesner, R. A.; Banks, J. L.; Murphy, R. B.; Halgren, T. A.; Klicic, J. J.; Mainz, D. T.; Repasky, M. P.; Knoll, E. H.; Shelley, M.; Perry, J. K.; Shaw, D. E.; Francis, P.; Shenkin, P. S. Glide: A new approach for rapid, accurate docking and scoring. 1. method and assessment of docking accuracy. *J. Med. Chem.* **2004**, *47*, 1739–1749.

(33) Friesner, R. A.; Murphy, R. B.; Repasky, M. P.; Frye, L. L.; Greenwood, J. R.; Halgren, T. A.; Sanschagrin, P. C.; Mainz, D. T. Extra precision glide: Docking and scoring incorporating a model of hydrophobic enclosure for protein-ligand complexes. *J. Med. Chem.* **2006**, *49*, 6177–6196.

(34) Mulliken, R. S. Electronic population analysis on LCAO-MO [linear combination of atomic orbital-molecular orbital] molecular wave functions. I. *J. Chem. Phys.* **1955**, *23*, 1833–1840.

(35) Cioslowski, J. A new population analysis based on atomic polar tensors. *J. Am. Chem. Soc.* **1989**, *111*, 8333–8336.

(36) Dewar, M. J. S.; Jie, C.; Zoebisch, E. G. AM1 calculations for compounds containing boron. *Organometallics* **1988**, *7*, 513–521.

(37) Dewar, M. J. S.; Zoebisch, E. G.; Healy, E. F.; Stewart, J. J. P. Development and use of quantum mechanical molecular models. 76. AM1: a new general purpose quantum mechanical molecular model. *J. Am. Chem. Soc.* **1985**, *107*, 3902–3909.

(38) Chandrasekhar, J.; Andrade, J. G.; Schleyer, P. V. R. Efficient and accurate calculation of anion proton affinities. *J. Am. Chem. Soc.* **1981**, *103*, 5609–5612.

(39) Clark, T.; Chandrasekhar, J.; Spitznagel, G. W.; Schleyer, P. V. R. Efficient diffuse function-augmented basis sets for anion calculations. III. The 3-21 + G basis set for first-row elements, lithium to fluorine. *J. Comput. Chem.* **1983**, *4*, 294–301.

(40) Fox, M. A.; Goeta, A. E.; Howard, J. A.; Hughes, A. K.; Johnson, A. L.; Keen, D. A.; Wade, K.; Wilson, C. C. The molecular structure of (PSH^+)(nido-7,8-$C_2B_9H_{12}$-) determined by neutron diffraction (PS = proton sponge, 1,8-bis(dimethylamino)naphthalene). *Inorg. Chem.* **2001**, *40*, 173–175.

(41) Cole, J. C.; Murray, C. W.; Nissink, J. W.; Taylor, R. D.; Taylor, R. Comparing protein-ligand docking programs is difficult. *Proteins* **2005**, *60*, 325–332.

(42) Holt, P. A.; Chaires, J. B.; Trent, J. O. Molecular docking of intercalators and groove-binders to nucleic acids using AutoDock and Surflex. *J. Chem. Inf. Model.* **2008**, *48*, 1602–1615.

(43) Fanfrlik, J.; Hnyk, D.; Lepsik, M.; Hobza, P. Interaction of heteroboranes with biomolecules. Part 2. The effect of various metal vertices and exo-substitutions. *Phys. Chem. Chem. Phys.* **2007**, *9*, 2085–2093.

(44) Fanfrlik, J.; Lepsik, M.; Horinek, D.; Havlas, Z.; Hobza, P. Interaction of carboranes with biomolecules: formation of dihydrogen bonds. *ChemPhysChem* **2006**, *7*, 1100–1105.

(45) Otkidach, D. S.; Pletnev, I. V. Conformational analysis of boron-containing compounds using Gillespie-Kepert version of molecular mechanics. *THEOCHEM* **2001**, *536*, 65–72.

(46) Esposito, E. X.; Baran, K.; Kelly, K.; Madura, J. D. Docking of sulfonamides to carbonic anhydrase II and IV. *J. Mol. Graphics Modell.* **2000**, *18* (283−289), 307–288.

(47) *MOE (The Molecular Operating Environment), version 2007.09*; Chemical Computing Group Inc.: Montreal, Canada H3A 2R7, 2007.

(48) Warren, G. L.; Andrews, C. W.; Capelli, A. M.; Clarke, B.; LaLonde, J.; Lambert, M. H.; Lindvall, M.; Nevins, N.; Semus, S. F.; Senger, S.; Tedesco, G.; Wall, I. D.; Woolven, J. M.; Peishoff, C. E.; Head, M. S. A critical assessment of docking programs and scoring functions. *J. Med. Chem.* **2006**, *49*, 5912–5931.

(49) Johnsamuel, J.; Byun, Y.; Jones, T. P.; Endo, Y.; Tjarks, W. A convenient method for the computer-aided molecular design of carborane containing compounds. *Bioorg. Med. Chem. Lett.* **2003**, *13*, 3213–3216.

CI900031Y